Kinetics of oxygen evolution at α-Fe₂O₃ photoanodes: a study by photoelectrochemical impedance spectroscopy

K.G. Upul Wijayantha^a, Sina Saremi-Yarahmadi^a and Laurence M. Peter^b*

Received (in XXX, XXX) Xth XXXXXXXXX 200X, Accepted Xth XXXXXXXX 200X First published on the web Xth XXXXXXXX 200X

DOI: 10.1039/b000000x

Photoelectrochemical Impedance Spectroscopy (PEIS) has been used to characterize the kinetics of electron transfer and recombination taking place during oxygen evolution at illuminated polycrystalline α-Fe₂O₃ electrodes prepared by aerosol-assisted chemical vapour deposition from a ferrocene precursor. The PEIS results were analysed using a phenomenological approach since the mechanism of the oxygen evolution reaction is not known a priori. The results indicate that the photocurrent onset potential is strongly affected by Fermi level pinning since the rate constant for surface recombination is almost constant in this potential region. The phenomenological rate constant for electron transfer was found to increase with potential, suggesting that the potential drop in the Helmholtz layer influences the activation energy for the oxygen evolution process. The PEIS analysis also shows that the limiting factor determining the performance of the α-Fe₂O₃ photoanode is electron -hole recombination in the bulk of the oxide.

Introduction

Several decades after the pioneering work of Fujishima and Honda¹ on water splitting at illuminated titanium dioxide crystals, efficient photoelectrochemical water splitting using semiconductor electrodes remains an important target. Early studies identified haematite (\alpha-Fe_2O_3) as potential photoanode material for water splitting²⁻⁴, and recent work has focussed on developing films that could be used as part of tandem photoelectrolysis cells⁵, in which high energy photons are used to drive the oxidation of water by photogenerated holes at the Fe₂O₃ surface, and lower energy photons transmitted through the oxide are harvested by a solar cell that applies a bias voltage to the photoelectrolysis cell. The photoelectrochemical properties of single crystal^{2, 6,} 7 and polycrystalline $^{8\text{--}10}$ $\alpha\text{-Fe}_2O_3$ photoanodes have been studied extensively, and recent optimization of the morphology and doping of nanostructured thin films of Fe₂O₃ have resulted in substantial improvements in the photocurrent response. 10-12 However, further work is needed before haematite electrodes can be considered for high efficiency water splitting.

Losses due to bulk and surface recombination of photogenerated electron hole pairs play a key role in determining the efficiency of photoelectrodes such as α -Fe₂O₃. 13, 14 The low mobility and short lifetime of holes combined with the high doping levels in Fe₂O₃ films lead to poor collection of holes from the bulk of the material to the surface. The problem of the short hole diffusion length $L_{\rm p}$ in

α-Fe₂O₃ has been addressed by fabricating nanostructured films in which the characteristic dimensions are comparable with L_p , so that holes have an increased chance of reaching the surface. However, even in the case where holes are collected efficiently in the space charge region and transferred to the interface, hole transfer leading to the oxidation of water has to compete with surface recombination of holes with electrons, which are majority carriers in the *n*-type oxide. Recombination may also occur in the space charge region.¹⁵ Little is known currently about the kinetics of these competing processes in the case of α -Fe₂O₃.

The mechanism of photoelectrochemical oxygen evolution on α-Fe₂O₃ must involve the transfer of 4 electrons per molecule of O₂ formed, but almost nothing is known about the individual elementary steps in the reaction. It is reasonable to suppose that the reaction steps in the oxygen evolution reaction involve higher-valent states of iron formed at the surface by hole capture. Schemes such as

$$\begin{aligned} hv &\rightarrow h^{+} + e^{-} \\ Fe(III)_{surf} + h^{+} &\rightarrow Fe(IV)_{surf} \\ Fe(IV)_{surf} + h^{+} &\rightarrow Fe(V)_{surf} \\ 2Fe(V) + 2 &H_{2}O \rightarrow 2 &Fe(III) + O_{2} + 4H^{+} \end{aligned}$$

illustrate the complications arising from the fact that the oxidation of water is a 4-electron process, so that holes need to be 'stored' in intermediate states.. The Fe(IV) and Fe(V) intermediates in this scheme can also act as electron acceptors, so that surface recombination reactions of the following kind are likely to take place.

$$Fe(IV) + e^{-} \rightarrow Fe(III)$$

$$Fe(V) + e^{-} \rightarrow Fe(IV)$$
Scheme 2

The Fe(IV) and Fe(V) states can also be thought of as 'surface-trapped holes', which may have sufficient surface mobility to allow second order reactions of the type illustrated by the last step shown in Scheme 1. Complex multistep reaction schemes of this type have been considered for reactions such as the photo-dissolution of silicon in fluoride electrolytes¹⁶ and the photo-decomposition of CdS¹⁷. The rate expressions derived from these kinetic schemes are generally rather cumbersome, since they include rate constants and surface concentrations for all of the intermediates and reaction steps. It is therefore more convenient to adopt a simpler phenomenological approach for the analysis of experimental data. The rate constants obtained from such an analysis can then be related to the expressions derived for different multistep reaction mecahnisms. 18 Here we show how this approach can be used to analyze data obtained by photoelectrochemical impedance spectroscopy (PEIS). The results provide new information about the rate constants for the competing processes that determine the performance of α-Fe₂O₃ photoanodes.

Theory

The simplest phenomenological scheme to describe the competition between charge transfer and recombination at an illuminated n-type semiconductor is illustrated in Fig.1. It has been assumed that electron transfer and recombination involve surface states (in principle, these can be the intermediates in the reaction schemes described above). Competition between the overall rates of hole transfer and recombination determines the fraction of the hole current j_i that is measured in the external circuit. This fraction corresponds to the internal quantum efficiency of the process.

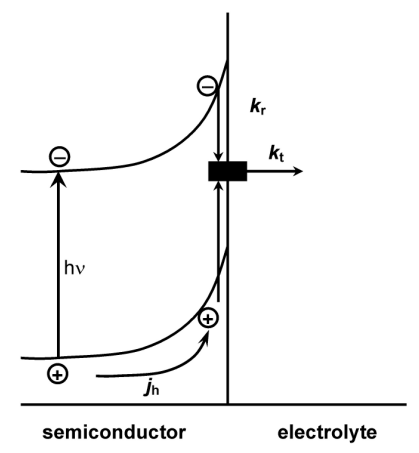


Fig 1 Phenomenological kinetic scheme for PEIS analysis

The scheme shown in Fig. 1 is a simplified version of the model used in our previous discussions of the phenomenological approach¹⁸ and its application to photoelectrochemical impedance spectroscopy (PEIS)^{17, 19} since it excludes direct hole transfer from the valence band to

solution redox species. This simplification is clearly appropriate in the absence of a one-electron redox couple in the electrolyte, The phenomenological first order rate constants k_t and k_r (s⁻¹) appearing in Fig. 1 and in the equations for the PEIS response are used to express the rate of hole transfer and recombination (cm⁻² s⁻¹) in terms of the surface concentration of 'trapped holes' (cm⁻²). If we take Scheme 1 and Scheme 2 as an example of a possible mechanism, the surface trapped holes correspond to Fe(IV) and Fe(V) species. 'Hole transfer' in this formalism therefore corresponds to the overall 4electron oxidation process leading to the formation of oxygen. Similarly the recombination process corresponds to electron capture by Fe(IV) and Fe(V) species, which can be thought of as photogenerated surface recombination centres. The rate of the recombination process depends on the electron capture cross sections and surface concentrations of Fe(IV) and Fe(V) species ('trapped holes') as well as on the concentration of free electrons available at the surface. It follows that k_r should depend on band bending $q\Delta\phi$, since the electron concentration at the surface is given by $n_{x=0} = n_{\text{bulk}} \exp(-q\Delta\phi/k_{\text{B}}T)$, where n_{bulk} is determined by the doping density, For highly doped semiconductors like Fe₂O₃ recombination may also involve electron tunnelling through the space charge region.

For the case where the Helmholtz capacitance is larger than the space charge capacitance, it has been shown that the impedance of the illuminated electrode is given by 19

$$Z = R_{ser} + \frac{1}{i\omega C_{sc} + \left(\frac{q}{k_B T}\right) j_h \frac{k_r}{k_t + k_r} \frac{k_t + i\omega}{k_t + k_r + i\omega}}$$
(1)

(It is shown below that this approximation is valid for the electrodes used in the present study). Here R_{ser} is the series resistance, $C_{\rm sc}$ is the space charge capacitance, $j_{\rm h}$ is the current density corresponding to the flux of holes reaching the interface. k_t and k_r are the first order rate constants for interfacial transfer and recombination respectively (cf. Fig. 1). The impedance described by equation 1 corresponds to two semicircles in the complex plane. The low frequency semicircle tends towards a zero frequency intercept on the real axis given by

$$Z_{1} = R_{ser} + \frac{k_{t} + k_{r}}{\left(\frac{q}{k_{B}T}\right)j_{h}k_{r}} \left(1 + \frac{k_{r}}{k_{t}}\right)$$

$$\tag{2}$$

The radial frequency $\omega_{max}(LF)$ corresponding to the maximum imaginary component of the low frequency semicircle is equal The high frequency limit of the low frequency to k_{t} . semicircle is

$$Z_{2} = R_{ser} + \frac{k_{t} + k_{r}}{\alpha \left(\frac{q}{k_{B}T}\right) j_{h} k_{r}}$$
(3)

It follows that

$$\frac{Z_1 - R_{ser}}{Z_2 - R_{cer}} = 1 + \frac{k_r}{k_r} \tag{4}$$

and

$$j_h = \frac{k_t + k_r}{\alpha \left(\frac{q}{k_n T}\right) k_r \left(Z_2 - R_{ser}\right)}$$
 (5)

The radial frequency $\omega_{\rm max}({\rm HF})$ corresponding to the maximum imaginary component of the high frequency semicircle is given by $1/[C_{\rm sc}(Z_2-R_{\rm ser})]$.

In the case of moderately-doped single crystal semiconductors, j_h approaches qI_0 , where I_0 is the incident photon flux (corrected for reflection loss). However, in the case of polycrystalline highly doped semiconductors like Fe_2O_3 , j_h is expected to be smaller than qI_0 , since electronhole pairs generated outside the space charge region are mostly lost by recombination. In addition, electronhole recombination in the space charge region may also reduce j_h .

It can be seen from this set of equations that k_t , k_r , C_{sc} and j_h can be determined experimentally from the PEIS response shown schematically in Fig. 2.

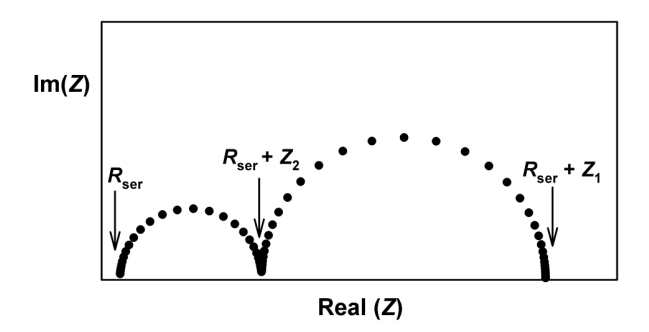


Fig 2 Typical PEIS response predicted by equation 1

This treatment of the data represents the simplest approach that does not require *a priori* knowledge of any parameters. More general expressions for the PEIS response that apply for the case where the space charge capacitance is not smaller than the Helmholtz capacitance and which also include the effects of surface state capacitance as well as the possibility that k_t is influenced by the potential drop in the Helmholtz layer can be found in the comprehensive extension of our original treatment by Leng et al. ²⁰ We have not used these expressions here since they include additional parameters with unknown values. It should be noted, however, that equation 18 given by Leng at al. for the case where $C_{\rm sc}$ is comparable with the Helmholtz capacitance corrects a typographical error in our original paper. ¹⁹

Experimental

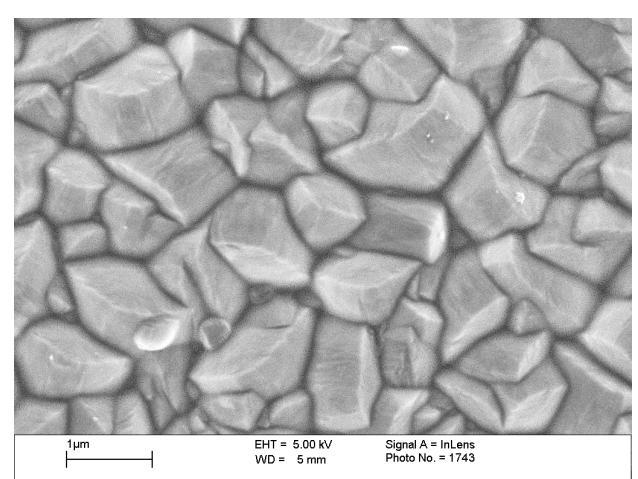
 $\alpha\text{-Fe}_2\mathrm{O}_3$ electrodes were deposited by aerosol-assisted chemical vapour deposition (AACVD) on fluorine-doped tin oxide coated glass substrates (FTO - TEC 8 Pilkington, 8 Ω square). Substrates were cleaned ultrasonically with distilled

water, acetone, isopropanol and ethanol. Details of the AACVD system are described elsewhere. Ferrocene (Fe(C_5H_5)₂, 98%, Lancaster Synthesis) was used as precursor. In a typical deposition, a 0.05 M solution of ferrocene in toluene was used to generate the aerosol at room temperature using an air humidifier. Air at a flow rate of 150 ml/min was used as the carrier gas, and the flow rate was controlled by a thermal mass flow controller (Bronkhorst UK Ltd.). FTO substrates (1cm × 2cm) were placed inside the reactor tube which was located in a tube furnace. The substrates were then heated at 450 °C for 20 min before starting the deposition. Deposition was maintained for 45 minutes. A strip at one end of the FTO substrate was masked by a glass microscope slide to prevent Fe₂O₃ deposition so that electrical contacts could be made for the electrochemical and photoelectrochemical measurements.

Impedance and photoelectrochemical measurements of hematite electrodes in 1 M NaOH electrolyte were conducted using a three-electrode cell, with Ag/AgCl/KCl reference electrode and a platinum wire counter electrode. Impedance and voltammetric experiments were performed using a computer-controlled potentiostat (AutoLab, PGSTAT12). For PEIS and steady-state I-V measurements, the Fe₂O₃ electrode was illuminated through electrolyte side with collimated blue light from an LED ($\lambda = 455$ nm. Thorlabs Ltd. UK). The illumination area was 1 cm². Intensity dependant PEIS studies were performed by attenuating the LED beam with neutral density filters (Knight Optical Ltd, UK). PEIS spectra were fitted to the R(RC)(RC) network corresponding to the response shown in Fig. 2. Incident photon to electron conversion efficiency (IPCE) spectra were obtained using a 75 W xenon lamp with a grating monochromator (TMc300, Bentham Instruments Ltd., UK). The light intensity was calibrated using a silicon diode.

Results and Discussion

The morphology of the Fe₂O₃ films is illustrated by the SEM pictures in Fig. 3. It can be seen that the surface of the films consists of well-formed crystallites with lateral dimensions of the order of 0.5 to 1.0 microns. The cross section shows evidence of columnar crystal growth. The films appear to be non-porous, and they are considerably thicker than those prepared from the ferrocene precursor in our previous work11. compared The relatively smooth morphology nanostructured films is convenient for this study since it avoids complications associated with three-dimensional development of the space charge region.²²



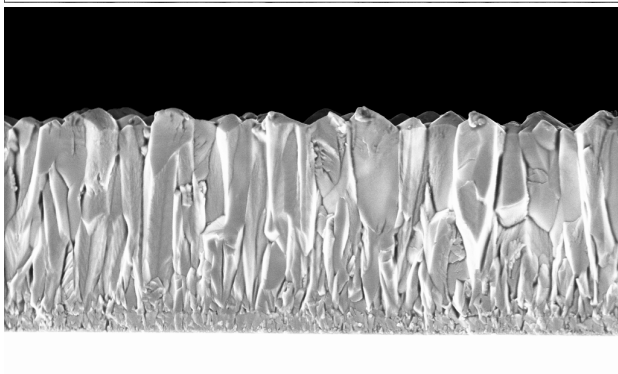


Fig 3. SEMs showing surface morphology and cross section of α-Fe₂O₃ films

Signal A = InLens Photo No. = 1741

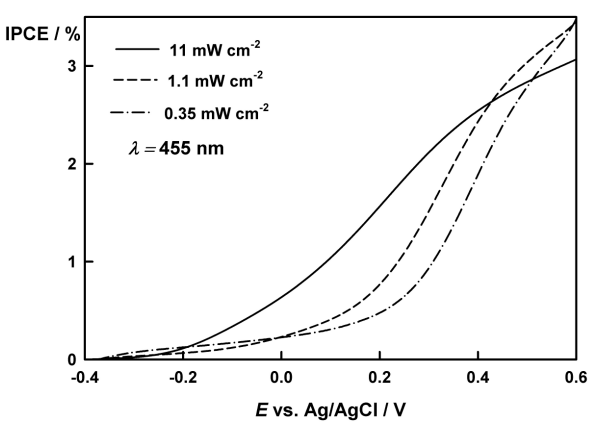
EHT = 5.00 kV

1µm ———

The peak IPCE of the α-Fe₂O₃ films at 350 nm is 13% at 0.23 V vs. Ag|AgCl, which is lower than the values for thinner nanostructured films. The PEIS measurements were carried out at longer wavelengths (455 nm), where the IPCE is around 2%. Normalised photocurrent voltage plots for three different light intensities are shown in Fig. 4. The low IPCE values suggest that the majority of electron-hole pairs are generated outside the space charge region and recombine. If recombination in the space charge region is negligible, the IPCE is given by

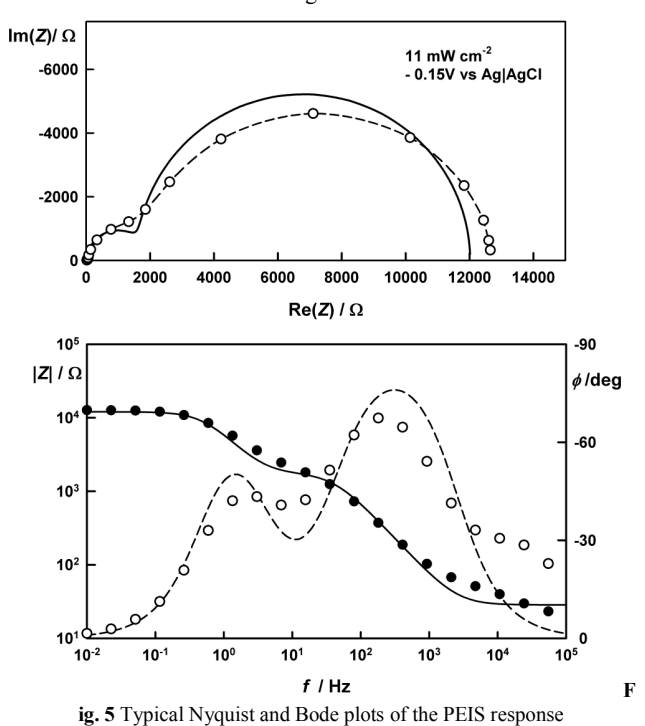
$$IPCE = (1 - R)(1 - e^{-\alpha W})$$
 (6)

where R is the reflection coefficient, α is the absorption coefficient and W is the width of the space charge region. Using the value $\alpha = 1.5 \times 10^5$ cm⁻¹ at 455 nm taken from the spectrum for $\alpha\text{-Fe}_2O_3$ films reported by Marusak et al. 23 gives a value of W of less than 200 nm at 0.4 V vs Ag|AgCl, which corresponds to a band bending of around 1 eV (reported values the flatband potential of Fe₂O₃ in 1.0 M NaOH lie in the range -0.5 V to -0.7 V vs. Ag|AgCl. $^{6,\,24}$ This means that the penetration depth of the light $(1/\alpha)$ is ca. 30 times larger than the width of the space charge region.



ig 4. Normalized photocurrent (IPCE) voltage curves recorded at 3 light intensities (455 nm LED illumination)

It can be seen from Fig. 4 that the normalized photocurrent in the range -0.4 to 0.4 V increases with illumination intensity so that the photocurrent onset shifts towards more negative There are several possible reasons for this potentials. including space charge²⁵ behaviour, and recombination²⁶⁻²⁸ as well as the kinetics of the multi-electron transfer process. 17, 18 The presence of surface recombination in this potential region can be deduced from the spikes and overshoot in the photocurrent response to chopped illumination (the transient photocurrent response of anodic Fe₂O₃ films on iron has been discussed in one of our early papers²⁹). For this reason, PEIS measurements were carried out in the onset region to obtain information about the competition between hole transfer and recombination. The same dc illumination intensities as those noted in Fig. 3 were used.



The measured PEIS responses generally showed the two semicircles predicted by equation 1. An example with the fitting is shown in Fig. 5. The flattening of the PEIS response that is evident in the Nyquist plot is similar to the PEIS response of p-InP19 and n-CdS17 electrodes reported elsewhere. In principle, a better fit can be obtained using a constant phase shift element, but since this approach complicates the analysis, it was not used. The effect may arise from a dispersion of kinetic parameters or from dispersion in the dielectric constant of Fe₂O₃ which has been reported in the literature.30

PEIS spectra were fitted and analyzed to obtain $k_{\rm t}, k_{\rm r}, C_{\rm sc}$ and j_h as a function of potential at three light intensities. Fig. 6 illustrates a set of data obtained at 1.1 mW cm⁻².

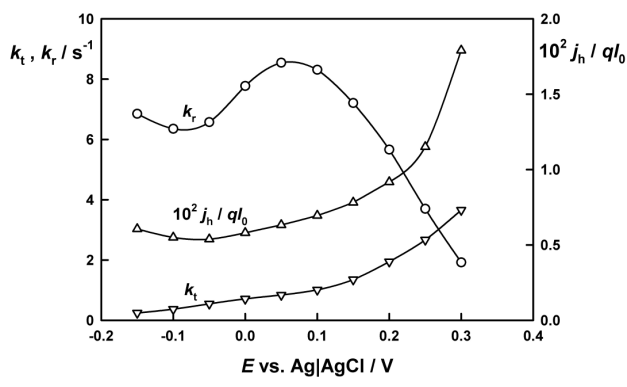


Fig. 6 The rate constants for charge transfer and recombination (k_t and $k_{\rm r}$) and the normalised hole flux derived from the analysis of PEIS spectra. dc illumination intensity 1.1 mW cm⁻². Note that the right hand scale corresponds to the IPCE that would be measured in the absence of surface recombination

The variation of the recombination rate constant k_r with potential indicates that the semiconductor/electrolyte junction is not behaving ideally. k_r depends linearly on the surface electron concentration n_{surf} , which for an ideal semiconductor/ electrolyte junction decreases by a factor of 10 per 59 meV of increased band bending. The plot of k_r vs. potential passes through a maximum before falling as expected for increasing band bending. This indicates that the band bending varies little over the initial potential range behaviour that is typical for Fermi level pinning associated with a high density of surface states. This conclusion is supported by impedance studies of single crystal α-Fe₂O₃ which have demonstrated the presence of surface states.⁶ As we show below, it appears as if the surface states are photoinduced in the present case, and the most likely explanation is that they are associated with higher valent iron species formed by hole capture.

The increase with potential of k_t , the rate constant for electron transfer, differs from the behaviour observed in more ideal systems, where k_t is found to be independent of potential.³¹ Since the increase in k_t with potential is observed in the potential range where Fermi level pinning occurs and the majority of the change in potential appears as a voltage across the Helmholtz layer, we assume that it indicates that the phenomenological rate constant for oxygen evolution is influenced by the potential drop across the Helmholtz layer in the same way as at a metal electrode, i.e. by modifying the free energy of the transition state.

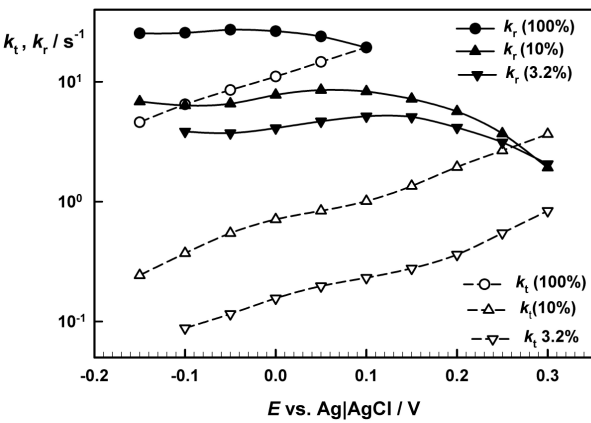
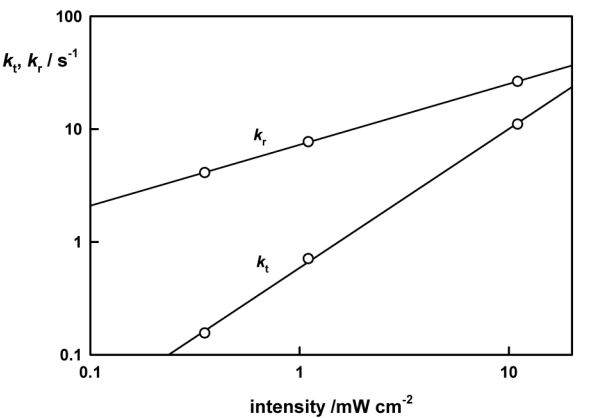


Fig.7 Dependence of k_t and k_r on potential for three light intensities

Fig. 7 contrasts the k_t and k_r values obtained from the analysis of PEIS spectra measured for three different illumination intensities. A logarithmic y scale has been chosen to show that the variation of k_t with potential corresponds to a Tafel slope of ca. 350 mV/decade for all three intensities. Tafel slopes for oxygen evolution of thin passivating Fe₂O₃ films on iron in the dark has been reported by Lyons and Brandon to lie in the range 40-50 mV. The weaker potential dependence in the present case may be related to the lower fraction of the overall potential drop that appears across the Helmholtz layer.



ig 8 Double logarithmic plots showing the intensity dependence of k_1 and k_2 . . Values measured at 0 V vs Ag|AgCl (cf. Fig. 7)

Both k_t and k_r depend on light intensity, with k_t varying more strongly with intensity than k_r . The variation of k_t and k_r with intensity is illustrated in the double logarithmic plot shown in Fig. 8. The values of the rate constants were taken from Fig. 7 at a potential of 0 V vs. Ag|AgCl. It can be seen from Fig. 8 that $k_{\rm T}$ varies with $I_0^{0.54}$, which is close to a square root dependence. By contrast k_t varies with $I_0^{1.2}$ which is close to a linear dependence. In principle these intensity dependencies could be related to possible mechanisms of the oxygen evolution, but such a treatment lies outside the scope of the present paper, which is restricted to the phenomenological approach.

The different intensity dependences explain why the photocurrent onset moves towards more negative potentials with increasing light intensity: the fraction of the hole flux that is consumed in the oxygen evolution reaction as opposed to recombination is determined by the ratio $k_t/(k_t + k_r)$, which has been plotted as a function of potential in Fig. 9. The validity of the analysis is demonstrated by the fact that the plots in Fig. 9 mirror the photocurrent voltage plots in Fig. 4. It is therefore clear that the delayed photocurrent onset can be attributed to surface recombination and Fermi level pinning. In order to overcome this problem, it will be necessary to remove the kinetic bottleneck that leads to the build up of intermediates that 'metallize' the surface and promote recombination by capturing electrons.

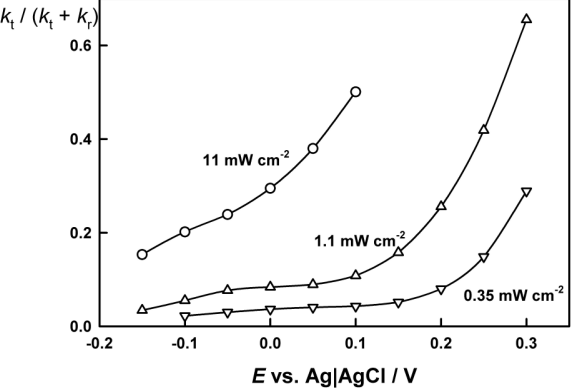


Fig. 9 The ratio $k_t / (k_t + k_r)$ as a function of potential for different light intensities. Compare with the current voltage plots in Fig. 4

The values of $C_{\rm sc}$ derived for the three light intensities from the PEIS analysis are plotted in Fig.10 in the form of Mott Schottky plots of $1/{C_{\rm sc}}^2$ vs. potential. The lines have been added as guides to the eye. The capacitance values are sufficiently small to justify the assumptions implicit in the derivation of equation 1. The plateau sections in the plots are consistent with the potential dependence of k_r since they indicate that Fermi level pinning occurs over a substantial part of the potential range. The dependence of the apparent flatband potential on light intensity follows the same trend as seen in the photocurrent voltage plots in Fig. 4, with the lowest intensity data showing the largest positive displacement along the voltage axis.

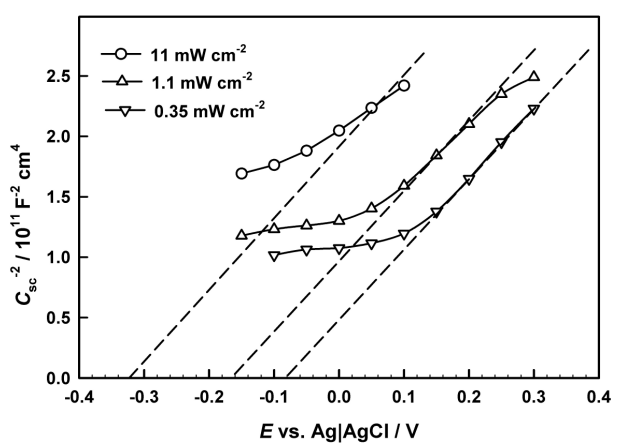


Fig. 10. Mott Schottky plots constructed using $C_{\rm sc}$ values derived from the PEIS analysis

The flatband potential derived from Mott Schottky plots of the dark capacitance (not shown) is around -0.6 V vs.

Ag|AgCl, so the displacement seen in the Mott Schottky plot for 0.35 mW cm^{-2} is 0.5 V. If a value of $20 \mu F \text{ cm}^{-2}$ is assumed for the Helmholtz capacitance, a shift of 0.5 V would correspond to a positive surface charge of 10⁻⁵ C cm⁻², i.e. to a surface 'hole' density of 6×10^{13} cm⁻². Such a large value would indicate that a substantial fraction of the Fe(III) sites on the surface of the $\alpha\text{-Fe}_2O_3$ electrode are converted under illumination to higher valent Fe species that are intermediates in the oxygen evolution reaction. However, this calculation is based on the assumption that the shifts in the Mott Schottky plots are due entirely to stored electronic charge and not to changes in ionic surface charge. This assumption is tested below (cf. Fig. 12).

Fig. 11 compares the normalised plots of j_h obtained from the analysis of PEIS data obtained at the three light intensities. It is evident that the normalised hole current densities are very similar. The values also agree well with the IPCE measured at 455 nm.

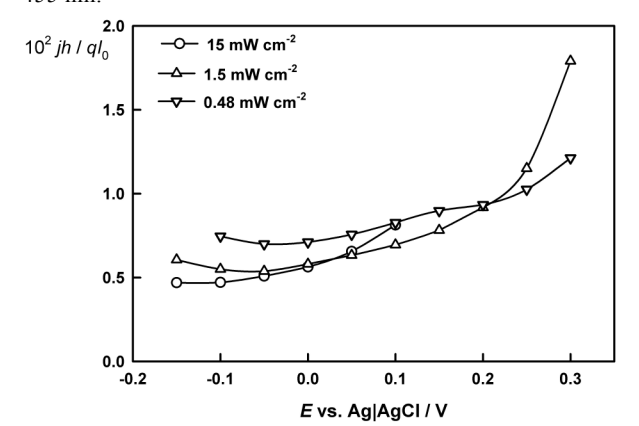


Fig. 11 Plots of hole current density j_h derived from the PEIS analysis and normalized to the incident photon flux for three light intensities

The photocurrent measured in the external circuit is expected to be equal to j_h , multiplied by the fraction $k_t/(k_t + k_r)$ of holes that are transferred in the oxygen evolution reaction. At more positive potentials where k_t becomes larger than k_r , the two current densities should become identical. Comparison of Figures 4 and 11 confirms that this is indeed the case. It follows that surface recombination mainly affects the photocurrent onset potential, whereas recombination in the volume of the electrode (i.e. in the quasi-neutral region and possibly also in the space charge region) determines the photocurrent at more positive potentials where the increase in photocurrent is due to widening of the space charge region.

We can test the hypothesis that the displacement of the Mott Schottky plots is due to the build up of positive surface charge corresponding to 'trapped holes' that are queuing to take part in the oxygen evolution reaction. The steady state build up of surface intermediates (represented by the surface concentration of 'trapped hole', p_{surf}) under illumination can be estimated from the hole flux into the surface and the rate constants for removal of 'surface trapped holes", k_t and k_r .

$$p_{surf} = \frac{j_h}{q(k_r + k_t)} \tag{7}$$

Fig. 12 illustrates the trapped hole charge that is derived for the three intensities from the PEIS analysis.

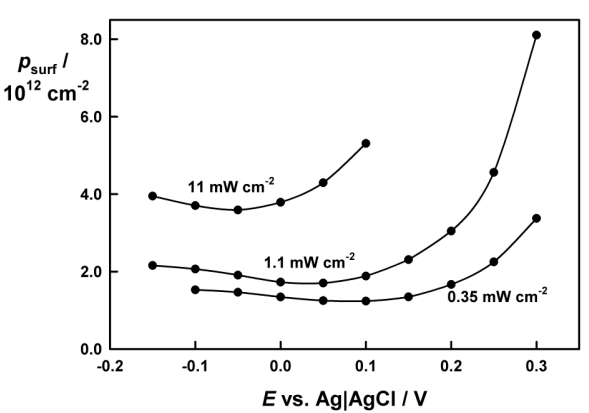


Fig. 12 . Surface hole concentrations as a function of potential calculated from equation 7 for three light intensities

The trapped hole densities derived from this approach are at least an order of magnitude lower than those estimated from the shift in flatband potential evident in the Mott Schottky plots. Furthermore the highest trapped hole density is calculated for the highest light intensity. If the displacement of the Mott Schottky plots were due simply to the trapped hole density, one would expect the order of the plots shown in Fig. 10 to be reversed. We therefore conclude tentatively that the shifts seen in Fig. 10 cannot arise from trapped holes. pH changes are unlikely to be important in 1 M NaOH, and in any case accumulation of protons near the surface during oxygen evolution would move the flatband potential to more positive values. An alternative possibility is that partial oxidation of the Fe(III) sites on the surface of the oxide changes the surface ionic charge as a consequence of different acid/base properties of the higher oxidation states of iron

Conclusions

This study has shown that electrochemical impedance spectroscopy can provide information phenomenological rate constants describing the competition between charge transfer and recombination during light driven oxidation of water at semiconductor electrodes. The complex potential dependence of the rate constants for these two processes highlights the non-ideal nature of the α-Fe₂O₃eletrolyte interface arsing from photogenerated surface Efficient water splitting in a tandem photoelectrochemical cell using α-Fe₂O₃ as a photoanode requires that the photocurrent onset should be as close to the flatband potential as possible, i.e. ideally near -0. 6 V vs. Ag|AgCl in 1.0 M NaOH., which is ca. 0.8 V negative of the reversible oxygen electrode potential. A positive displacement of the photocurrent onset represents a loss of free energy and hence of efficiency. Clearly this means that accumulation of positive surface charge associated with Fermi level pinning and changes in surface composition must be avoided as far as possible. Since the accumulation of electronic and ionic surface charge appears to be associated with sluggish hole transfer kinetics, it should be possible to

overcome the effects by using a suitable surface catalyst for the oxygen evolution reaction. At the same time, the loss of holes by recombination in the bulk of the semiconductor needs to be minimized. This can be achieved at least in part by growing nanostructured thin films in such a way that the dimensions are comparable with the width of the space charge region.^{32, 33} Other promising approaches include using oriented nanorod arrays³⁴ or a host-guest structure in which small α-Fe₂O₃ particles are deposited on a porous oxide substrate such as WO₃.35 The present results, which were obtained for relatively flat non-optimized α-Fe₂O₃ films, indicate the utility of PEIS for the characterization of kinetic of the water splitting systems. Work is in progress to characterize the photoelectrochemical oxidation of water at illuminated α-Fe₂O₃ electrodes using intensity modulated photocurrent spectroscopy (IMPS), which can yield complementary information. 17, 19

Acknowledgments

KGUW and SSY acknowlege support from EPSRC and Loughborough University Materials Research School.

References

- 1. A. Fujishima and K. Honda, Nature, 1972, 238, 37-38.
- J. H. Kennedy and K. W. Frese, J. Electrochem. Soc., 1977, 124, C130-C130.
- J. H. Kennedy and M. Anderman, J. Electrochem. Soc., 1983, 130, 848-852.
- R. K. Quinn, R. D. Nasby and R. J. Baughman, *Mat. Res. Bull.*, 1976, 11, 1011-1017
- E. Pollert, J. Hejtmanek, J. P. Doumerc, J. C. Launay and P. Hagenmuller, Z. Anorg.. Allg. Chem., 1985, 528, 202-208.
- M. S. Antonious, H. Makram, M. Herlem and M. Etman, C. R. Acad. Sci. ser. h, 302, 549-552.
- M. P. Dare-Edwards, J. B. Goodenough, A. Hamnett and P. R. Trevellick, J. Chem. Soc.-Faraday Trans. I, 1983, 79, 2027-2041.
- A. Kay, I. Cesar and M. Grätzel, J. Am. Chem. Soc., 2006, 128, 15714-15721.
- I. Cesar, K. Sivula, A. Kay, R. Zboril and M. Grätzel, *J. Phys. Chem.* C, 2009, 113, 772-782.
- S. Saremi-Yarahmadi, A. A. Tahir, B. Vaidhyanathan and K. G. U. Wijayantha, *Mater. Lett.*, 2009, 63, 523-526.
- S. Saremi-Yarahmadi, K. G. U. Wijayantha, A. A. Tahir and B. Vaidhyanathan, J. Phys. Chem. C, 2009, 113, 4768-4778.
- W. J. Albery, P. N. Bartlett, A. Hamnett and M. P. Dare-Edwards, J. *Electrochem. Soc.*, 1981, 128, 1492-1501.
- P. Lemasson, J. Gautron, W. J. Albery, P. N. Bartlett, M. P. Dareedwards and A. Hamnett, *J. Electrochem. Soc.*, 1982, 129, 1269-1270.
- P. T. Landsberg, Recombination in Semiconductors, Cambridge University Press, Cambridge, 1991.

^a Department of Chemistry, University of Loughborough, Loughborough LE11 3TU, United Kingdom. Tel: +44(0)1509 22574; E-mail: U. Wijayantha @lboro.ac.uk

^b Department of Chemistry, University of Bath, Bath BA2 7AY, United Kingdom. Tel: +44 (0)1225 368502 E-mail:l.m.peter@bath.ac.uk

- 15. W. J. Albery and P. N. Bartlett, J. Electrochem. Soc., 1983, 130,
- 16. L. M. Peter, A. M. Borazio, H. J. Lewerenz and J. Stumper, J. Electroanal. Chem., 1990, 290, 229-248.
- 17. D. J. Fermin, E. A. Ponomarev and L. M. Peter, J. Electroanal. Chem., 1999, 473, 192-203.
- 18. L. M. Peter, E. A. Ponomarev and D. J. Fermin, J. Electroanal. Chem., 1997, 427, 79-96.
- 19. E. A. Ponomarev and L. M. Peter, J. Electroanal. Chem., 1995, 396, 219-226.
- 20. G. Schlichthörl, E. A. Ponomarev and L. M. Peter, J. Electrochem. Soc., 1995, 142, 3062-3067.
- 21. G. Schlichthörl, E. A. Ponomarev and L. M. Peter, J. Electrochem. Soc., 1995, 142, 3062-3067.
- 22. W. H. Leng, Z. Zhang, J. Q. Zhang and C. N. Cao, J. Phys. Chem. B, 2005, **109**, 15008-15023.
- 23. A. A. Tahir, K. G. U. Wijayantha, S. Saremi-Yarahmadi, M. Mazhar and V. McKee, Chem. Mater., 2009, 21, 3763-3772.
- 24. L. A. Marusak, R. Messier and W. B. White, J. Phys. Chem. Solids, 1980, 41, 981-984.
- 25. S. U. M. Khan and J. Akikusa, J. Phys. Chem. B, 1999, 103, 7184-
- 26. D. Vanmaekelbergh and F. Cardon, Semicond. Sci. Technol., 1988, **3**, 124-133.
- 27. L. M. Peter, J. Li and R. Peat, J. Electroanal. Chem., 1984, 165, 29-
- 28. J. Li, R. Peat and L. M. Peter, J. Electroanal. Chem., 1984, 165, 41-59.
- 29. L. M. Abrantes and L. M. Peter, J. Electroanal. Chem., 1983, 150,
- 30. E. A. Ponomarev and L. M. Peter, J. Electroanal. Chem., 1995, 397,
- 31. J. C. Papaioannou, G. S. Patermarakis and H. S. Karayianni, J. Phys. Chem. Solids, 2005, 66, 839-844.
- 32. F. Le Formal, M. Grätzel and K. Sivula, Adv. Funct. Mat., 20, 1099-
- 33. J. Brillet, M. Grätzel and K. Sivula, Nano Letters, 10, 4155-4160.
- 34. R. van de Krol, Y. Q. Liang and J. Schoonman, J. Mater. Chem., 2008, 18, 2311-2320.
- 35. K. Sivula, F. Le Formal and M. Grätzel, Chem. Mater., 2009, 21, 2862-2867.

- 1. A. Fujishima and K. Honda, Nature, 1972, 238, 37-+.
- R. K. Quinn, R. D. Nasby and R. J. Baughman, Materials Research Bulletin, 1976, 11, 1011-1017.
- J. H. Kennedy and K. W. Frese, Journal of the Electrochemical 3. Society, 1977, 124, C130-C130.
- 4. J. H. Kennedy and K. W. Frese, Journal of the Electrochemical Society, 1978, 125, 709-714.
- 10 5. J. Brillet, M. Cornuz, F. Le Formal, J. H. Yum, M. Gratzel and K. Sivula, Journal of Materials Research, 25, 17-24.
 - M. P. Dareedwards, J. B. Goodenough, A. Hamnett and P. R. Trevellick, Journal of the Chemical Society-Faraday *Transactions I*, 1983, **79**, 2027-2041.
- 15 7. E. Pollert, J. Hejtmanek, J. P. Doumerc, J. C. Launay and P. Hagenmuller, Zeitschrift Fur Anorganische Und Allgemeine Chemie, 1985, 528, 202-208.
 - A. G. Agrios, I. Cesar, P. Comte, M. K. Nazeeruddin and M. Gratzel, Chemistry of Materials, 2006, 18, 5395-5397.
- 20 9. I. Cesar, A. Kay, J. A. G. Martinez and M. Gratzel, Journal of the American Chemical Society, 2006, 128, 4582-4583.
 - 10. A. Kay, I. Cesar and M. Gratzel, Journal of the American Chemical Society, 2006, 128, 15714-15721.
- 11. S. Saremi-Yarahmadi, A. A. Tahir, B. Vaidhyanathan and K. G. U. Wijayantha, Materials Letters, 2009, 63, 523-526.
- 12. S. Saremi-Yarahmadi, K. G. U. Wijayantha, A. A. Tahir and B. Vaidhyanathan, Journal of Physical Chemistry C, 2009, 113, 4768-4778.
- 13. W. J. Albery, P. N. Bartlett, A. Hamnett and M. P. Dareedwards, Journal of the Electrochemical Society, 1981, 128, 1492-1501.
- 14. P. Lemasson, J. Gautron, W. J. Albery, P. N. Bartlett, M. P. Dareedwards and A. Hamnett, Journal of the Electrochemical Society, 1982, 129, 1269-1270.
- 15. P. T. Landsberg, Recombination in Semiconductors, Cambridge University Press, Cambridge, 1991.
- 16. L. M. Peter, A. M. Borazio, H. J. Lewerenz and J. Stumper, J. Electroanal. Chem. Interfacial Electrochem., 1990, 290, 229-
- 17. D. J. Fermin, E. A. Ponomarev and L. M. Peter, Journal of Electroanalytical Chemistry, 1999, 473, 192-203.
- 18. L. M. Peter, E. A. Ponomarev and D. J. Fermin, Journal of Electroanalytical Chemistry, 1997, 427, 79-96.
- 19. E. A. Ponomarev and L. M. Peter, J. Electroanal. Chem., 1995, 397, 45-52
- 45 20. W. H. Leng, Z. Zhang, J. Q. Zhang and C. N. Cao, Journal of Physical Chemistry B, 2005, 109, 15008-15023.
 - 21. A. A. Tahir, K. G. U. Wijayantha, S. Saremi-Yarahmadi, M. Mazhar and V. McKee, Chemistry of Materials, 2009, 21, 3763-3772.
- 22. I. Cesar, K. Sivula, A. Kay, R. Zboril and M. Graetzel, Journal of Physical Chemistry C, 2009, 113, 772-782.
- 23. L. A. Marusak, R. Messier and W. B. White, Journal of Physics and Chemistry of Solids, 1980, 41, 981-984.
- 24. S. U. M. Khan and J. Akikusa, Journal of Physical Chemistry B, 1999, 103, 7184-7189.
- 55 25. D. Vanmaekelbergh and F. Cardon, Semiconductor Science and Technology, 1988, 3, 124-133.

- 26. L. M. Peter, J. Li and R. Peat, J. Electroanal. Chem. Interfacial Electrochem., 1984, 165, 29-40.
- 27. J. Li, R. Peat and L. M. Peter, J. Electroanal. Chem. Interfacial Electrochem., 1984, 165, 41-59.
- 28. J. Li and L. M. Peter, J. Electroanal. Chem. Interfacial Electrochem., 1985, 193, 27-47.
- 29. L. M. Abrantes and L. M. Peter, Journal of Electroanalytical Chemistry, 1983, 150, 593-601.
- 65 30. J. C. Papaioannou, G. S. Patermarakis and H. S. Karayianni, Journal of Physics and Chemistry of Solids, 2005, 66, 839-844.
- 31. G. Schlichthoerl, E. A. Ponomarev and L. M. Peter, J. Electrochem. Soc., 1995, 142, 3062-3067.
- 32. F. Le Formal, M. Gratzel and K. Sivula, Advanced Functional Materials, 20, 1099-1107.
- 33. J. Brillet, M. Gratzel and K. Sivula, Nano Letters, 10, 4155-4160.
- 34. R. van de Krol, Y. Q. Liang and J. Schoonman, Journal of Materials Chemistry, 2008, 18, 2311-2320.
- 35. K. Sivula, F. Le Formal and M. Gratzel, Chemistry of Materials, 2009, 21, 2862-2867.